Vol.64: e21190760, 2021
https://doi.org/10.1590/1678-4324-2021190760
ISSN 1678-4324 Online Edition

Article - Agriculture, Agribusiness and Biotechnology

Can the Granulometric Soil Fractions Attenuate the Radiation Differently from the Whole Soil?

Luis Valério Prandel[1]*
https://orcid.org/0000-0002-5807-8738

André Maurício Brinatti[1]
https://orcid.org/0000-0001-5625-3865

Sérgio da Costa Saab[1]
https://orcid.org/0000-0003-3842-8574

Luiz Fernando Pires[1]
https://orcid.org/0000-0001-5073-5900

Larissa Macedo dos Santos Tonial[2]
https://orcid.org/0000-0002-5307-9379

[1]State University of Ponta Grossa (UEPG), Ponta Grossa, Paraná, Brazil; [2]Federal Technological University of Paraná, Pato Branco, Paraná, Brazil.

Editor-in-Chief: Paulo Vitor Farago
Associate Editor: Andressa Novatski

Received: 2019.12.18; Accepted: 2020.10.07.

*Correspondence:luisprandel@gmail.com; Tel.: +55-42-32203044 (L.V.P.).

HIGHLIGHTS

- Semi-quantitative elemental analysis of the soils was accomplished through EDXRF.
- The μ, PA, CS and IS of hardsetting soil fractions was calculated by using the XCOM computer code.
- The mineralogical composition was determined by the RM-XRD.
- With PCA was possible to discriminate soil fractions and to correlate μ, PA, CS and IS.

Abstract: The purpose of this research was to discriminate soil fractions using mineralogical and elemental analyses and to show those fractions that present greater contribution to the soil mass attenuation coefficient (μ) as well as their partial cross-sections for photoelectric absorption (PA), coherent scattering (CS) and incoherent scattering (IS). Soil samples from different places of Brazil classified as Yellow Argisol, Yellow Latosol and Gray Argisol were submitted to elemental and mineralogical analyses through energy dispersive X-ray fluorescence (EDXRF) and Rietveld Method with X-ray diffraction data (RM-XRD). The mixture rule was utilized to calculate μ of each soil. The EDXRF analysis showed as predominant elements Si, Al, Fe and Ti oxides. The highest contents were Si (914.3 to 981.3 g kg^{-1}) in the sand fractions, Al (507.9 to 543.7 g kg^{-1}) and Fe (32.5 to 76.7 g kg^{-1}) in the clay fractions, and Ti (18.0 to 59.0 g kg^{-1}) in the silt fractions. The RM-XRD allowed identifying that the sand fractions are predominantly made of quartz (913.3 to 995.0 g kg^{-1}), while the clay greatest portion is made of kaolinite (465.0 to 660.6 g kg^{-1}) and halloysite (169.0 to 385.0 g kg^{-1}). The main effect responsible for μ was IS (50 to 61.4%) followed by PA (28 to 40.1%) and CS (9.9 to 10.6%). By using the principal component analysis (PC-1: 57.5% and PC-2: 20.9%), the samples were differentiated through the discrimination between physical, chemical and mineralogical properties. The results obtained suggest that general information about the radiation interaction in soils can be obtained through the elemental and mineralogical analyses of their fractions.

Keywords: mass attenuation coefficient; XCOM; principal component analysis; Rietveld method; partial cross-Sections.

GRAPHICAL ABSTRACT

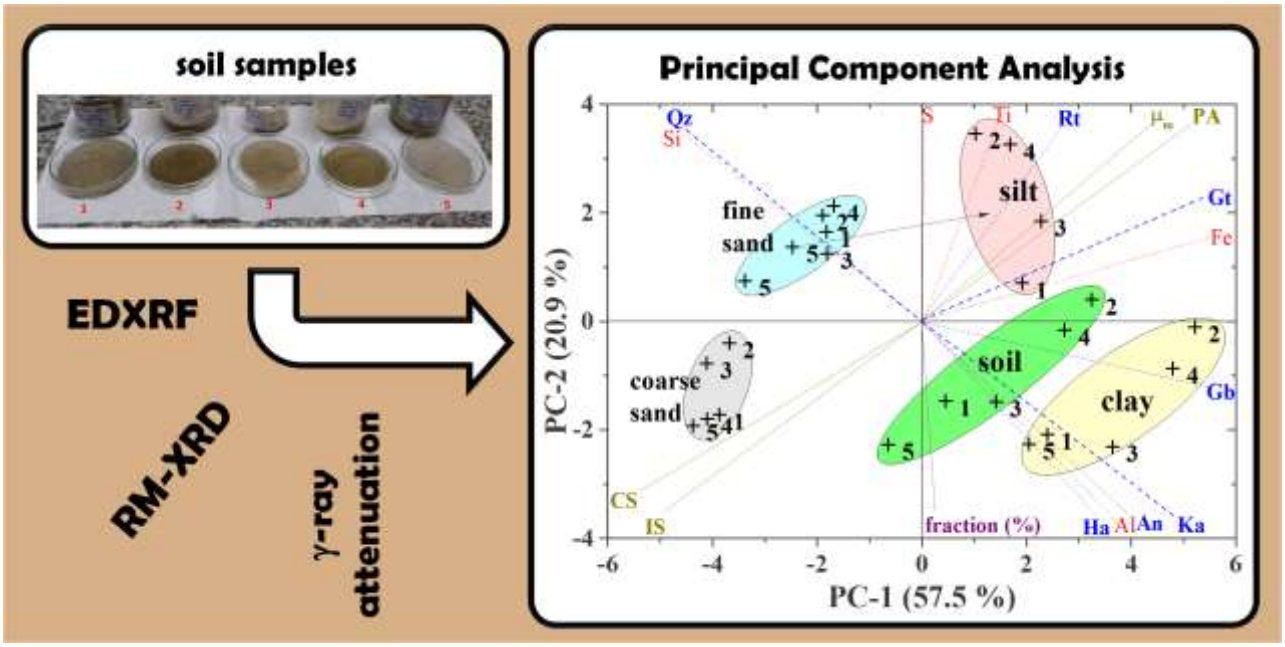

INTRODUCTION

The comprehension of how radiation interacts with different materials is crucial in fundamental physics as well as in many other applied fields [1,2]. In the environmental physics field many radiation parameters of the soil have been utilized for the measurement of properties such water retention, water movement, connectivity and tortuosity of the pores and so on [3,4]. The determination of soil radiation parameters requires the evaluation of its chemical composition by analytical techniques or direct measurements [1-3].

Soils as well as their granulometric fractions: coarse sand, fine sand, silt and clay can be characterized by employing different techniques of elemental analyses, the energy dispersive X-ray fluorescence (EDXRF) is among them [5-7]. The different soil granulometric fractions are also characterized by distinct mineralogical compositions [8]. A question that arises here is whether the soil granulometric fractions could influence the radiation interactions differently from the whole soil. The answer to this question can help the soil scientists in the development of new strategies for the characterization of soil properties and to understand the mechanisms of photon interaction with this complex porous media.

Mass attenuation coefficient (μ) as well as its partial cross-section for photoelectric absorption (PA), coherent scattering (CS) and incoherent scattering (IS) are the most important parameters to characterize the interaction of the radiation with the matter [9-11]. Pires and coauthors [12] used whole soil samples to correlate mineralogical results using the Rietveld Method with X-ray diffraction data (RM-XRD) and elemental results using EDXRF with μ analyses. These authors pointed out that not only the chemical composition of the soil influence μ, but also its mineralogical composition is important. The measurement of μ from the gamma photon radiation interaction in soils and their fractions, together with their mineralogical properties, is very relevant since it enables the prediction of physical properties such as bulk density, water content and total porosity [13-15].

As far as it is known, there are no studies correlating mineralogy results from RM-XRD and EDXRF elemental composition results from the soil fractions with μ, PA, CS and IS. However, to correlate a great amount of data with these techniques, it is necessary to employ statistical tools, such as Principal Component Multivariate Analysis (PCA) [16]. Nowadays, PCA has been applied to soils and their fractions for studies on organic matter [17], compaction and texture [18], mineralogy and elemental analysis [19,20], resulting in the efficient discrimination of samples that present a large number of variables.

Therefore, the analysis of the radiation attenuation parameters along with information about the soil mineralogical and elemental compositions can offer insights into how the granulometric fractions affect the attenuation properties of the soil [8]. Thus, the purpose of this research was to determine the influence of different soil fractions in some radiation attenuation properties. We also presented a theoretical analysis to show whether the radiation interactions in each granulometric fraction corroborate the total interactions in their respective soils.

MATERIAL AND METHODS

Soil samples

Brazilian soils (named s1 to s5), classified according to the Brazilian Soil Classification System [21], were collected and mixed in order to obtain a composite sample.

About 20 g of each sample was mashed and sieved (2 mm aperture sieve), dispersed, submitted to coarse sand separation (0.053 mm aperture sieve) and physical fractioning process by sedimentation (Stokes law) to extract the fine sand, silt and clay fractions; and the textural analysis was carried out by using the ratio between the fraction mass dried in an oven at 45 ºC and the total soil mass [6].

X-ray fluorescence and Rietveld Method using X-ray diffraction data

Semi-quantitative elemental analysis of the soils was accomplished through the EDXRF by using the instrument model EDX-720 (Shimadzu) equipped with an Rh X-ray tube. An X-ray Diffractometer, model Ultima IV (Rigaku), with CuK_{α} radiation, 40 kV voltage and 30 mA current was employed to collected data for MR-XRD analyses. Details about the experimental procedures can be found in Prandel and coauthors [6,22] and Pires and coauthors [12].

Gamma ray attenuation analysis

The μ, PA, CS and IS were obtained based on the soil elemental chemical composition through the XCOM software. In this study the XCOM software was selected due to its user-friendliness by utilizing the NIST-database service [23,24] and it can provide attenuation coefficients for the following processes: μ, PA, CS and IS in the field of the atomic nucleus and in the field of the atomic electrons [25].

Compound material μ can be calculated by using [26,27]:

$$\mu = \sum \mu_i w_i, \quad (1)$$

where μ_i is the mass attenuation coefficient of i^{th} element and w_i is the weight fraction of i^{th} element.

In this study the photon energy 59.5 keV (^{241}Am) was selected for the analysis of radiation interaction with the matter. The choice of this energy was based on the most common radioisotopes used as radioactive sources for gamma ray attenuation studies in soil science [28-30].

Principal component analysis

The variables related to the textural, elemental and mineralogical analyses, as well as μ, PA, CS and IS of the whole soil samples and their fractions were exported to a data matrix and correlated using the Principal Component Analysis (PCA). The raw data were auto scaled before calculation. The PCA was performed using Pirouette 4.5 software (Infometrix, USA).

The sample scores were represented by the coordinate of the first principal component (PC-1) and second principal component (PC-2), linearly dependent on their respective variables, represented by the loading axes.

RESULTS

Table 1 shows the textural analysis and elemental composition of the soils under study. The textural analysis revealed predominance of the coarse sand fraction (52.3 - 67.2%), followed by clay (28.4 to 43.9%), fine sand (2.2 to 3.8%) and silt (0.6 to 2.2%). The soil samples presented, based on the EDXRF elemental analysis, contents of Si, Al, Fe and Ti oxides as predominant, with the highest contents as follow: Si (914.3 to 981.3 g kg^{-1}) in the sand fractions; Al (507.9 to 543.7 g kg^{-1}) and Fe (32.5 to 76.7 g kg^{-1}) in the clay fractions; and Ti (18.0 to 59.0 g kg^{-1}) in the silt fractions. These contents are related to the minerals that make up these fractions. The S oxide content (1.4 to 15.9 g kg^{-1}), even being considerable in all fractions, was not a producer

of the minerals identified. The presence of Ca oxide (12.9 to 27.9 g kg^{-1}) in clay is due to the flocculating agent, $CaCl_2$, used in the physical fractioning process.

Table 1. Percentage (%) and EDXRF semi quantitative analysis of soils and their fractions (coarse sand, fine sand, silt and clay) [6].

Soil	C	F	P (%)	Oxides (g kg^{-1})					
				SiO_2	Al_2O_3	Fe_2O_3	TiO_2	CaO	SO_3
Yellow Argisol (s1)	Coruripe, Alagoas (10º07' S, 36º10' W)	wh	99.9 (6)	444 (4)	492 (7)	28.9 (6)	22.6 (4)	nd	10 (2)
		c. sand	62 (1)	974 (1)	nd	3.4 (1)	7.5 (1)	nd	1.4 (1)
		f. sand	2.4 (1)	927 (2)	nd	15 (1)	28.1 (3)	nd	15.9 (9)
		silt	2.2 (6)	583 (8)	317 (6)	35 (3)	48.1 (4)	nd	8.1 (4)
		clay	33.7 (3)	389 (2)	533 (4)	32.5 (8)	22.1 (4)	13 (2)	9 (1)
Yellow Latosol (s2)	Cruz das Almas, Bahia (12º40' S, 39º06' W)	wh	100.0 (3)	428 (4)	466 (7)	74 (2)	18.7 (5)	nd	11 (1)
		c. sand	64.2 (3)	970 (1)	nd	5.7 (1)	7.1 (1)	nd	14.3 (2)
		f. sand	2.9 (4)	924 (3)	nd	20.5 (5)	30.8 (9)	nd	16 (2)
		silt	0.9 (1)	884 (5)	nd	46 (3)	49 (4)	nd	14 (2)
		clay	32.1 (3)	373 (3)	507.9 (2)	77 (1)	16.2 (1)	16 (2)	8.9 (6)
Yellow Argisol (s3)	Porto Seguro, Bahia (16º27' S, 39º03' W)	wh	100.2 (3)	403 (5)	525 (6)	34.8 (7)	26.1 (5)	nd	8 (1)
		c. sand	52.3 (5)	981 (1)	nd	2.2 (1)	4.4 (1)	nd	10.8 (2)
		f. sand	2.4 (2)	916 (4)	nd	8.8 (5)	33 (1)	nd	16 (2)
		silt	1.7 (2)	616 (19)	278 (29)	30 (2)	51 (7)	nd	9 (1)
		clay	43.9 (3)	361 (5)	544 (6)	37 (1)	24.0 (7)	14.6 (5)	8 (1)
Yellow Argisol (s4)	Aracruz, Espírito Santo (19º49' S, 40º16' W)	wh	100.5 (1)	414 (3)	489 (3)	54.8 (3)	27.4 (5)	nd	11.5 (4)
		c. sand	52.9 (3)	956 (1)	nd	2.2 (1)	nd	nd	1.4 (2)
		f. sand	2.2 (1)	914 (5)	nd	18 (3)	34 (2)	nd	15 (3)
		silt	1.6 (1)	753 (3)	122 (3)	43 (2)	59 (3)	nd	10.9 (8)
		clay	43.9 (1)	378 (2)	514 (5)	54 (2)	24.9 (6)	18 (3)	9.3 (5)
Gray Argisol (s5)	Pacajus, Ceará (04º10' S, 3827' W)	wh	100.0 (4)	472 (3)	478 (4)	22.1 (6)	11.3 (3)	nd	10.2 (9)
		c. sand	67.2 (8)	981 (1)	nd	nd	nd	nd	1.6 (2)
		f. sand	3.8 (1)	952 (3)	nd	7.6 (8)	11.9 (6)	nd	14.0 (9)
		silt	0.6 (2)	938 (9)	nd	16 (6)	18 (3)	nd	15.1 (4)
		clay	28.4 (3)	404 (3)	507 (7)	25 (4)	11.8 (2)	28 (6)	9.2 (4)

C: Collect place; F: Fraction; P: mass percentage; wh: whole soil; c sand: coarse sand; f sand: fine sand; values between parentheses represent the standard deviation of the mean; nd: not detected.

Table 2 presents the content of minerals quantified using RM-XRD. Sand fractions (fine and coarse) are predominantly made of quartz (913.3 to 995.0 g kg^{-1}). The clay greatest portion is made of kaolinite (465.0 to 660.6 g kg^{-1}) and halloysite (169.0 to 385.0 g kg^{-1}). The goethite, anatase, gibbsite, rutile and quartz contents were seen in amounts lower than 80 g kg^{-1} in clays. In general, the silt samples presented high quartz content (403.0 to 949.7 g kg^{-1}), followed by kaolinite (41.0 to 660.6 g kg^{-1}) and other minerals (< 87.0 g kg^{-1}) that are present in clay.

Table 2. Mineral content using RM-XRD analysis of soils and their clay, silt and sand fractions [6].

Mineral	F	Mineral content (g kg^{-1})				
		Yellow Argisol (s1)	**Yellow Latosol (s2)**	**Yellow Ultisol (s3)**	**Yellow Argisol (s4)**	**Gray Ultisol (s5)**
Ka	wh	213.7	184.5	246.8	274.7	184.3
	c. sand	Nd	nd	nd	nd	nd
	f. sand	Nd	nd	nd	nd	nd
	silt	459.0 (1)	53.0 (1)	235.4 (6)	164.0 (2)	41.0 (1)
	clay	554.0 (1)	581.0 (1)	465.0 (1)	660.6 (9)	639.1 (7)
Gt	wh	18.9	33.0	15.0	25.8	nd
	c. sand	Nd	nd	10.3 (5)	15.5 (6)	nd
	f. sand	22.9 (8)	9.5 (7)	0.7 (2)	2.9 (7)	nd
	silt	1.8 (5)	18.0 (6)	73.8 (6)	4.7 (6)	nd
	clay	13.8 (5)	72.7 (9)	15.5 (5)	21.0 (8)	nd
An	wh	16.3	11.4	11.6	21.9	28.7
	c. sand	10.6 (7)	5.3 (5)	1.4 (3)	4.3 (5)	2.9 (1)
	f. sand	13.7 (6)	1.8 (5)	9.0 (5)	2.2 (4)	nd
	Silt	21.3 (6)	6.4 (4)	20.4 (6)	12.3 (5)	2.5 (3)
	clay	15.6 (3)	13.3 (5)	34.0 (3)	42.0 (1)	32.9 (7)
Gb	wh	22.9	44.5	61.1	22.0	1.4
	c. sand	Nd	nd	nd	nd	nd
	f. sand	Nd	3.3 (1)	75.6 (2)	6.0 (10)	0.7 (2)
	silt	19.0 (10)	30.0 (8)	31.7 (8)	14.0 (10)	nd
	clay	30.0 (7)	25.9 (8)	77.9 (9)	56.0 (20)	16.4 (9)
Ha	wh	72.5	42.3	107.8	81.6	44.6
	c. sand	Nd	nd	nd	nd	nd
	f. sand	5.7 (3)	nd	nd	17.0 (10)	nd
	silt	87.0 (10)	30.0 (10)	76.0 (20)	22.0 (20)	nd
	clay	373.0 (20)	258.0 (30)	385.0 (20)	169.0 (20)	227.0 (20)
Qz	wh	651.2	681.6	553.7	560.4	716.8
	c. sand	989.4 (3)	994.7 (1)	988.3 (1)	978.4 (1)	995.0 (1)
	f. sand	952.3 (1)	982.1 (1)	913.3 (3)	964.6 (2)	993.4 (0)
	silt	403.0 (10)	854.7 (3)	610.3 (8)	765.6 (7)	949.7 (1)
	clay	6.5 (3)	41.0 (10)	5.9 (4)	17.7 (8)	26.0 (6)
Rt	wh	3.1	1.5	2.3	9.0	3.1
	c. sand	Nd	nd	nd	nd	2.0 (1)
	f. sand	6.0 (10)	nd	nd	7.1 (7)	5.9 (4)
	silt	9.3 (4)	7.4 (4)	19.1 (5)	17.4 (6)	6.8 (4)
	clay	3.5 (3)	2.1 (3)	5.1 (4)	14.9 (7)	9.9 (4)

Ka: kaolinite; Gb: gibbsite; Qz: quartz; Rt: rutile; Gt: goethite; An: anatase; Ha: halloysite; F: Fraction; wh: whole soil; c sand: coarse sand; f sand: fine sand; values between parentheses represent the standard deviation of the mean; nd: not detected.

Figure 1 shows μ results and PA, CS and IS contributions regarding the γ photon energy 59.54 keV (^{241}Am). The highest μ and PA values were found in the clay fractions (0.2746 to 0.3064 cm^2 g^{-1} and 33.6 to 40.1 %, respectively) and silt (0.2699 to 0.2982 cm^2 g^{-1} and 35.8 to 38.2%, respectively), while the CS (10.5 to 10.6%) and IS effects (59.9 to 61.7%) were higher in the coarse sand. In all samples under analysis, the order of contribution to μ was IS>PA>CS. The different effects have distinct dependences of μ variation with photon energy. The region of low photon energies (<0.1 MeV) normally has great contributions of PA and CS, the former presents a probability of occurrence that increases for materials composed of heavy elements with an inverse relation with energy [2,8,10]. For the intermediate photon energies as those of ^{241}Am the dominant effect is IS, which is almost independent of Z. For IS, the number of electrons per gram is the most relevant factor that contributes the interaction of the radiation with the matter.

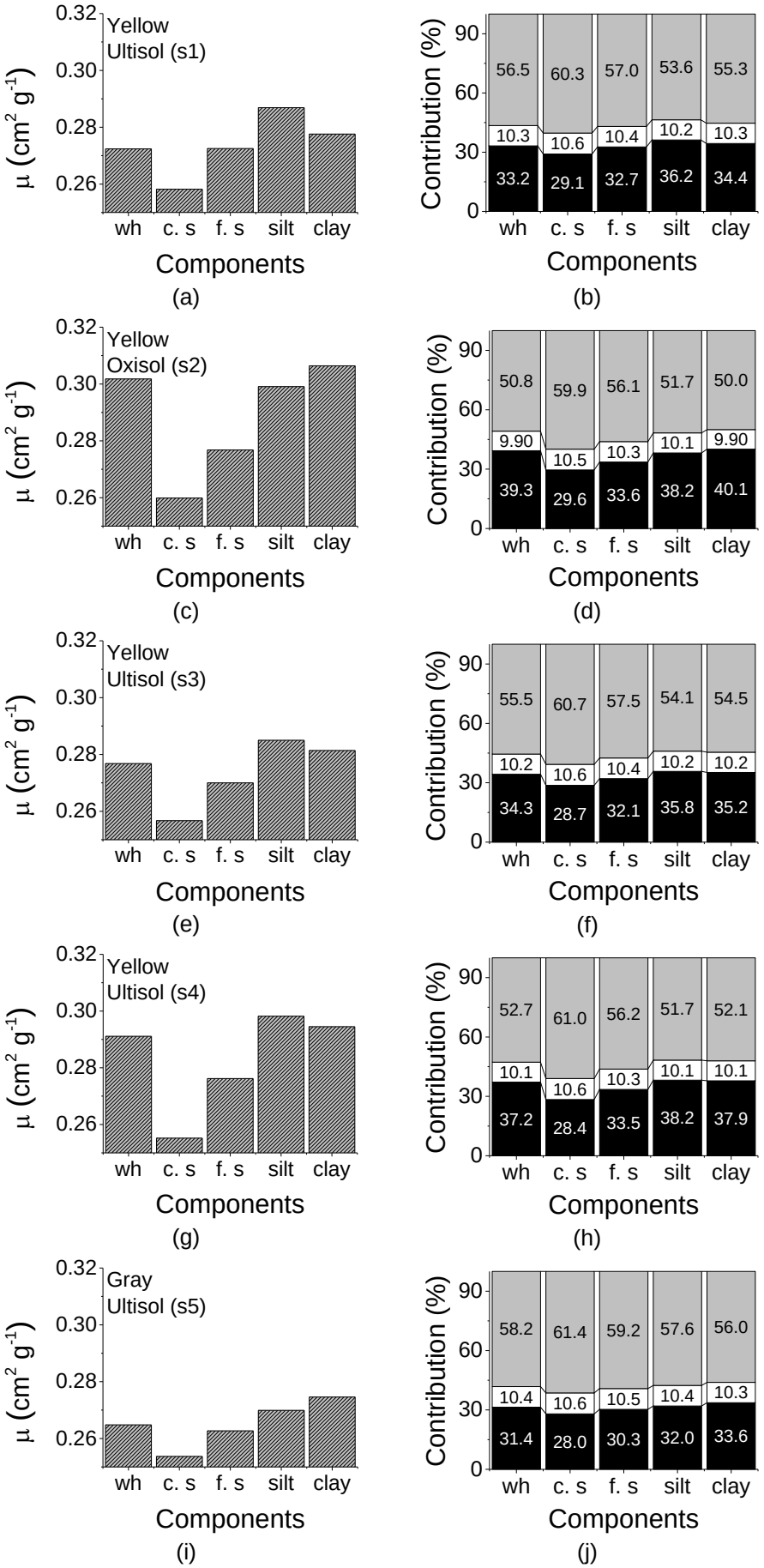

Figure 1. (a,b) Mass attenuation coefficient (μ, ▨) and the contribution of the photoelectric effect (PA, ■), coherent scattering (CS, ⊏) and incoherent scattering (IS, ■) for the Yellow Ultisol (s1), (c,d) Yellow Oxisol (s2), (e,f) Yellow Ultisol (s3), (g,h) Yellow Ultisol (s4), (i,j) Gray Ultisol (s5). wh: whole soil; c. s: coarse sand; f. s: fine sand.

The Figure 2 shows the PCA graph generated from the results of texture (mass percentage), and oxide content (Table 1), mineral percentage (Table 2), μ, PA, CS and IS (Figure 1) (totalling 17 variables and 25 samples) reducing the two principal components (PC-1 and PC-2), with a 78.4% total variance. The axes related to the loadings, full and broken lines indicate the trends in relation to the variables included in the PCA, that is, percentage of fractions, elements, minerals and attenuation coefficients, for each quadrant.

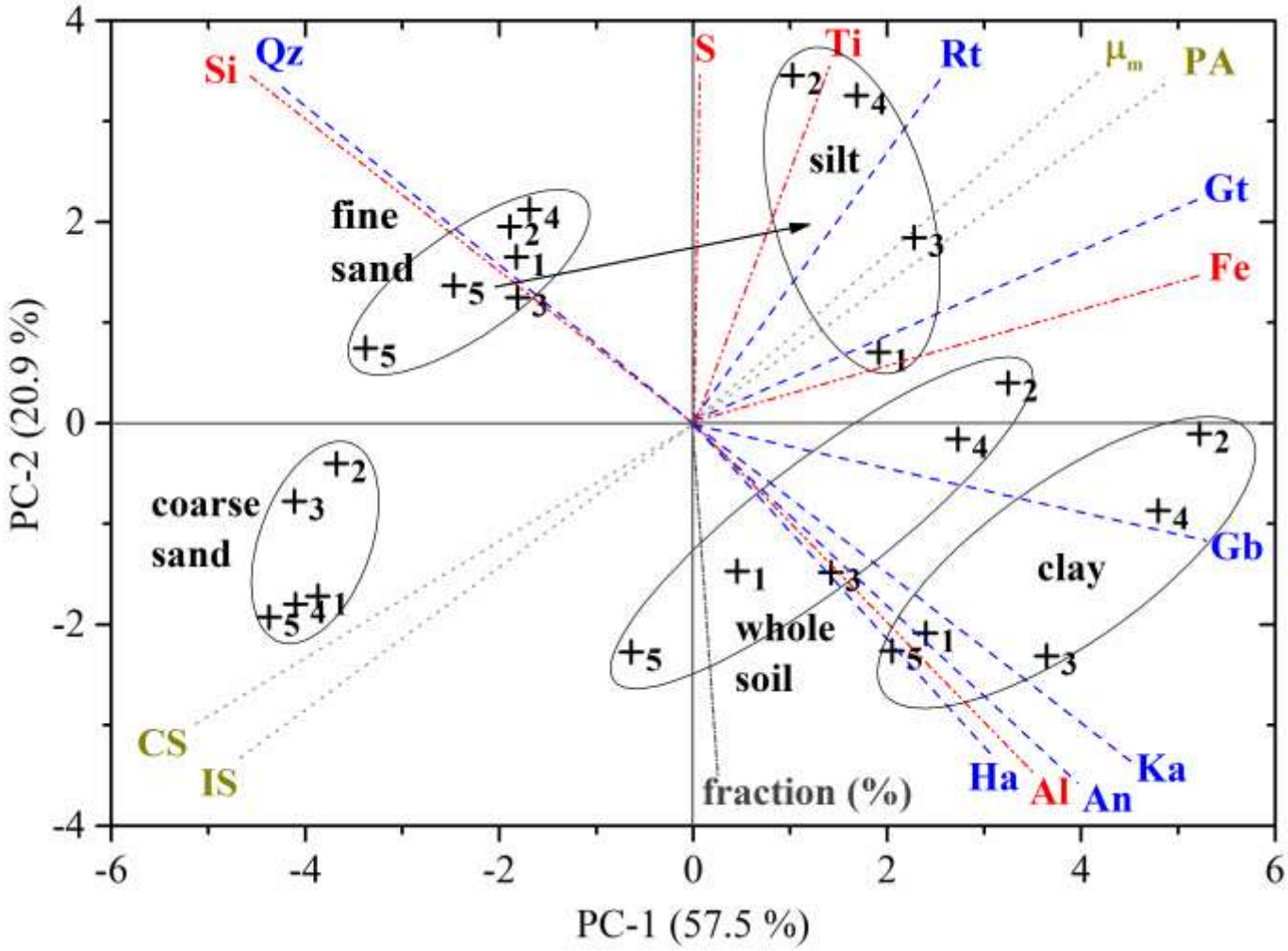

Figure 2. "Scores" of PC-1 and PC-2 of soil samples and their fractions with the inclusion of the following variables: texture, oxide content, mineral percentage, mass attenuation coefficient (μ), photoelectrical effect (PA), coherent (CS) and incoherent (IS) scattering. "Loadings" of the following trends: elements (full and broken lines), minerals (full lines), radiation interaction with the samples (broken lines). Key: kaolinite (Ka), gibbsite (Gb), quartz (Qz), rutile (Rt), goethite (Gt), anatase (An) and halloysite (Ha). The numbers close to the points represent the different soil types: s1 (1), s2 (2), s3 (3), s4 (4) and s5 (5).

The coarse sand, fine sand, silt and clay samples occupied distinct quadrants due to the discrimination between their physical, chemical and mineralogical properties. The point that represents the silt sample (s5) resembles the fine sand group, which is related to its Si and Qz content. The clay group was located in the lower right quadrant due to the presence of the minerals Ka, Ha, Gb and An, and the chemical element Al. The silt samples were grouped in the upper right quadrant influenced by the minerals Rt and Gt and the elements Ti and Fe.

The highest μ and PA were located in the upper right quadrant (Figure 2), which was influenced by the silt fraction. On the other hand, the coarse sand fraction (lower left quadrant) had lower effect in μ and PA. The chemical elements Fe and Ti presented higher influence in μ and PA in comparison to Si and Al. This is mainly caused by the Z^{4-5} dependency on PA [25].

The PA presented great influence in μ following the same sequence for the whole soil and the clay fraction: (s2) > (s4) > (s3) > (s1) > (s5) (Figures 1 and 2). In both cases, these effects were related to higher and lower Fe concentrations as goethite in the samples (s2) and (s5), respectively (Table 1). In the lower left quadrant (Figure 2), the coarse sand fraction, where quartz was the predominant mineral, was seen to be the most important factor influencing CS and IS [28,29]. The IS is related to the interaction of γ-ray photons

with the electronic layers, regardless of Z and it is directly proportional to the number of electrons per gram [10,12].

To prove whether the radiation interactions in each granulometric fraction corroborate the total interactions in their respective soils, proportionality relations between the μ, PA, CS and IS as a function of the weighted mean values (X_p) were determined by:

$$X_p = \frac{(p_{cs}x_{cs})+(p_{fs}x_{fs})+(p_s x_s)+(p_c x_c)}{p_{total}} \quad (2)$$

Where X_p takes the weighted values μ_p, PA_p, CS_p or IS_p (see Table 3); p_{cs}, p_{fs}, p_s and p_c are the coarse sand, fine sand, silt and clay contents obtained in the textural analysis, respectively; x_{cs}, x_{fs}, x_s and x_c are the percentage γ-ray interaction contribution (μ, PA, CS or IS) with the coarse sand, fine sand, silt and clay fractions; and p_{total} is the soil total amount, that is, the sum of each fraction content.

Table 3. Weighted mean values of the mass attenuation coefficient (μ_p) and the maximum (') and the minimum ('') values of μ calculated by equation (2) based on the standard deviation of the mean for the whole soil.

Soil	μ_p (cm² g⁻¹)	μ_p' (cm² g⁻¹)	μ_p'' (cm² g⁻¹)
Yellow Ultisol (s1)	0.2655	0.2700	0.2608
Yellow Oxisol (s2)	0.2759	0.2782	0.2736
Yellow Ultisol (s3)	0.2686	0.2710	0.2661
Yellow Ultisol (s4)	0.2738	0.2751	0.2724
Gray Ultisol (s5)	0.2601	0.2727	0.2574

Figure 3a,b show the μ graph as a function of μ_p (R^2 = 0.94) as well as the PA graph as a function of PA_p (R^2 = 0.91), respectively. The points are within the linear adjustments μ_p' and μ_p'', and PA_p' and PA_p'' (Figure 3a,b). The maximum (') and minimum ('') values of all the variables presented in Figure 3a-d were calculated (Equation 2) based on the standard deviation of the mean (Table 3). Thus, attenuation data for the fractions was seen to be reliable for having a direct dependence on their respective total values.

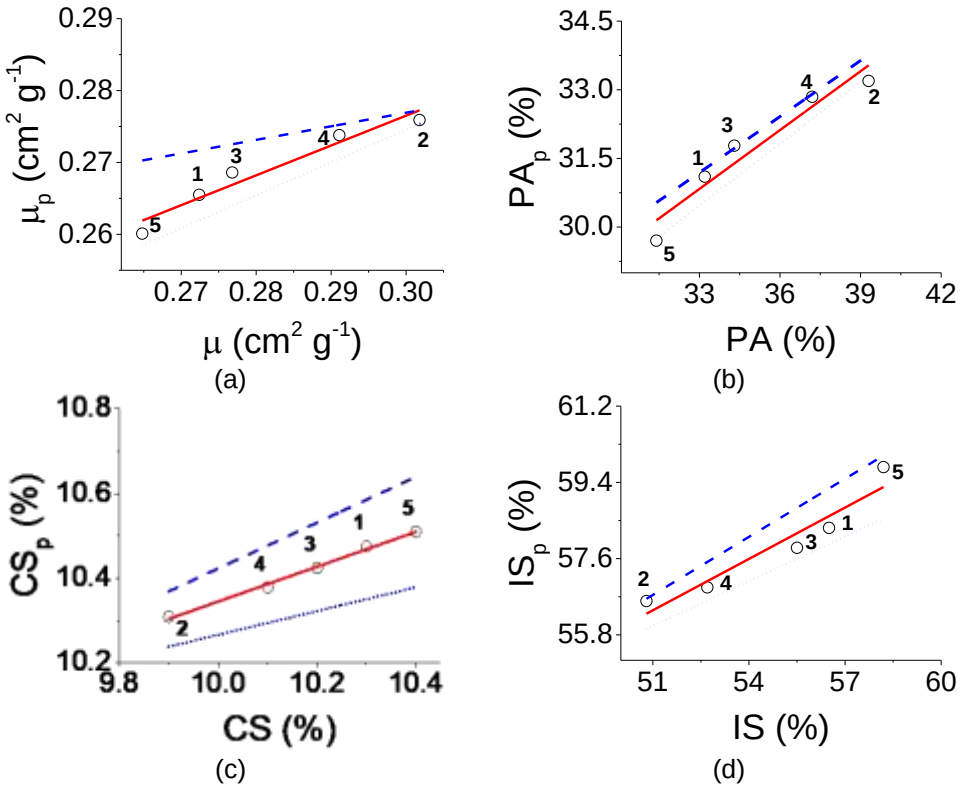

Figure 3. Linear adjustments of weighted means **(a)** μ_p **(b)** PA_p **(c)** CS_p **(d)** IS_p of granulometric fractions as a function of the mass attenuation coefficient (μ) and photoelectric effect (PA), coherent scattering (CS) and incoherent scattering (IS) contributions to μ of whole soil. The numbers close to the points (○) represent the different soil types: s1 (1), s2 (2), s3 (3), s4 (4) and s5 (5). The solid red line stands for the whole soil, the dash blue line for the maximum (') and the dot blue line for the minimum ('') values of all the variables calculated by equation (2) based on the standard deviation of the mean.

Figure 3 c,d show the CS (R^2 = 0.99) and the IS (R^2 = 0.89) linear adjustment graphs. The points of both adjustments are between CS_p' and CS_p'', and IS_p' and IS_p'', respectively. The results shown in Figure 3a-d are related to the proportionality relations of μ, PA, CS and IS and their weighted means (Equation 2) for each of the soil samples under study (s1-s5). In general, the results of Figure 3a-d revealed agreement between μ, PA, CS and IS of the whole soil and its respective weighted mean values; which were calculated from the radiation interaction with each fraction and their contents. Therefore, the general information about the radiation interaction for the whole soil can be obtained through its fractions.

CONCLUSION

The PCA enabled the discrimination of the soil fractions through mineralogical, elemental and textural analyses correlated with μ, PA, CS and IS. The contribution of the PA and μ followed the same proximity with order of contribution (s2) > (s4) > (s3) > (s1) > (s5) for the whole soils as well as the clay and silt fractions. These effects were related to Fe concentrations as the mineral goethite. However, CS and IS effects occurred with higher intensity in the coarse sand fraction, where quartz was the predominant mineral. The linear adjustments of weighted means (μ_p, PA_p, CS_p and IS_p) revealed that there is agreement between the calculated and estimated radiation interaction parameters (μ, PA, CS and IS) based on the soil fractions.

Acknowledgments: To Conselho Nacional de Desenvolvimento Científico e Tecnológico (CNPq) for the research grant and to Prof. Dr. Neyde Fabíola Balarezo Giarola for the soil sample supply.
Conflicts of Interest: "The authors declare no conflict of interest."

REFERENCES

1. Kurudirek M, Dogan B, Özdemir Y, Moreira AC, Appoloni CR. Analysis of some Earth, Moon and Mars samples in terms of gamma ray energy absorption buildup factors: Penetration depth, weight fraction of constituent elements and photon energy dependence. Radiat Phys Chem. 2011;80:354-64.
2. Kurudirek M. Estimation of effective atomic numbers of some solutions for photon energy absorption in the energy region 0.2–1.5 MeV: An alternative method. Nuclear Inst and Methods in Physics Research A. 2011;659:302-6.
3. Mayar MA, Schmid G, Wieprecht S, Noack M. Optimizing vertical profile measurements setup of gamma ray attenuation. Radiat Phys Chem. 2019;164:108376.
4. Galdos MV, Brown E, Rosolem CA, Pires LF, Hallett PD, Mooney SJ. Brachiaria species influence nitrate transport in soil modifying soil structure with their root system. Sci Rep. 2020;10:5072.
5. Melquiades FL, Thomaz EL. X-Ray Fluorescence to Estimate the Maximum Temperature Reached at Soil Surface during Experimental Slash-and-Burn Fires. J Environ Qual. 2016;45:1104-9.
6. Prandel LV, Saab SC, Brinatti AM, Giarola NFB, Leite WC, Cassaro FAM. Mineralogical analysis of clays in hardsetting soil horizons, by X-ray fluorescence and X-ray diffraction using Rietveld method. Radiat Phys Chem. 2014;95:65-8.
7. Pires LF, Prandel LV, Saab SC. The effect of wetting and drying cycles on soil chemical composition and their impact on bulk density evaluation: An analysis by using XCOM data and gamma-ray computed tomography. Geoderma. 2014;213:512-20.
8. Pires LF, Leite WC, Brinatti AM, Saab SC. Radiation attenuation properties based on the quantification of soil components using the Rietveld Method. Results Phys. 2019;12:2009-11.
9. Shams AM, Sayyed MI, Zaid MHM, Matori KA. Photon parameters for gamma-rays sensing properties of some oxide of lanthanides. Results Phys. 2018;9:206-10.
10. Medhat ME, Pires LF, Arthur RCJ. Analysis of photon interaction parameters as function of soil composition. J Radioanal Nucl Ch. 2014;300:1105-12.
11. Costa JC, Borges JAR, Pires LF, Arthur RCJ, Bacchi OOS. Soil mass attenuation coefficient: Analysis and evaluation. Ann Nucl Energy. 2014;64:206-11.
12. Pires LF, Brinatti AM, Prandel LV, Saab SC. Mineralogical composition of hardsetting soils and its effect on the radiation attenuation characteristics. J Soil Sediment. 2016;16:1059-68.
13. Borges JAR, Pires LF, Pereira AB. Computed tomography to estimate the representative elementary area for soil porosity measurements. Sci World J. 2012;2012:ID526380.
14. Elias EA, Bacchi OOS, Reichardt K. Alternative soil particle-size analysis by gamma-ray attenuation. Soil Till Res 1999;52:121-3.
15. Oliveira JCM, Appoloni CR, Coimbra MM, Reichardt K, Bacchi OOS, Ferraz E, Silva SC, Galvão Filho W. Soil structure evaluated by gamma-ray attenuation. Soil Till Res. 1998;48:127-33.
16. Johnson RA, Wichern DW. Applied multivariate statistical analysis. Upper Saddle River: Prentice hall; 2007. 773p.
17. Rossi CQ, Pereira MG, García AC, Berbara RLL, Gazolla PR, Perin A, González AP. Effects on the composition and structural properties of the humified organic matter of soil in sugarcane straw burning: A chronosequence study in the Brazilian Cerrado of Goiás State. Agr Ecosyst Environ. 2016;216:34-43.
18. Freddi OS, Ferraudo AS, Centurion JF. Multivariate analysis of a red latosol compaction cultivated with corn. Braz J Soil Sci. 2008;32:953-61.

19. Castilhos NDB, Melquiades FL, Thomaz EL, Bastos RO. X-ray fluorescence and gamma-ray spectrometry combined with multivariate analysis for topographic studies in agricultural soil. Appl Radiat Isotopes. 2015;95:63-71.
20. Melo VF, Barbar LC, Zamora PGP, Schaefer CE, Cordeiro GA. Chemical, physical and mineralogical characterization of soils from the Curitiba Metropolitan Region for forensic purpose. Forensic Sci Int. 2008;179:123-34.
21. Santos HG, Jacomine PKT, Anjos LHC, Oliveira VA, Oliveira JB, Coelho MR, Lumbreras JF, Cunha TJF. Sistema brasileiro de classificação de solos. Brasília: Embrapa;2013.353p.
22. Prandel LV, Dias NMP, Saab SC, Brinatti AM, Giarola NFB, Pires LF. Characterization of kaolinite in the hardsetting clay fraction using atomic force microscopy, X-ray diffraction, and the Rietveld method. J Soil Sediment. 2017;17:2144-55.
23. Mann KS, Rani A, Heer MS. Shielding behaviors of some polymer and plastic materials for gamma-rays. Radiat Phys Chem. 2015;106:247-54.
24. XCOM: Photon cross sections database - NIST Standard Reference Database 8 (XGAM). 2010. Available online: https://www.nist.gov/pml/xcom-photon-cross-sections-database (accessed on 22 jun 2016).
25. Kaplan I. Nuclear Physics. Vancouver: Addison-Wesley; 1963. 770p.
26. Costa JC, Borges JAR, Pires LF. Soil bulk density evaluated by gamma-ray attenuation: Analysis of system geometry. Soil Till Res. 2013;129:23-31.
27. Borges JAR, Pires LF. Representative elementary area (REA) in soil bulk density measurements through gamma ray computed tomography. Soil Till Res. 2012;123:43-9.
28. Medhat ME. Application of gamma-ray transmission method for study the properties of cultivated soil. Ann Nucl Energy. 2012;40:53-9.
29. Demir D, Ün A, Özgül M, Şahin Y. Determination of photon attenuation coefficient, porosity and field capacity of soil by gamma-ray transmission for 60, 356 and 662 keV gamma rays. Appl Radiat Isotopes. 2008;66:1834-7.
30. Lowenthal G, Airey PL. Practical applications of radioactivity and nuclear radiations. Cambridge: Cambridge University Press; 2001. 337p.